Predictive and interpretative modelling of ASDEX-Upgrade liquid metal divertor experiment

J. Cecrdle[1,2,3], J.G.A. Scholte[4], J. Horacek[1], T.W. Morgan[4,5], K. Krieger[6], H. Greuner[6], B. Böswirth[6], A. Manhard[6], D. Tskhakaya[1] M. Faitsch[6], and the ASDEX Upgrade Team

[1]Institute of Plasma Physics of the CAS, Za Slovankou 1782/3, 182 00 Prague 8, Czech Republic
[2]Department of Physics, Faculty of Nuclear Sciences and Physical Engineering, Czech Technical University in Prague, Brehova 78/7, 115 19 Prague, Czech Republic
[3]Department of Applied Physics, Ghent University, 9000 Ghent, Belgium
[4]Eindhoven University of Technology, Department of Applied Physics and Science Education, De Groene Loper 19,5312 AP Eindhoven, The Netherlands
[5]Dutch Institute for Fundamental Energy Research, De Zaale 20, 5612 AJ Eindhoven, The Netherlands
[6]Max Planck Institute für Plasma Physik, Boltzmannstr. 2, 85748 Garching, Germany
Corresponding author email: cecrdle@ipp.cas.cz

Keywords: Divertor, Liquid metal, ASDEX Upgrade, CPS

Abstract

A liquid metal Capillary Porous System (CPS) test module filled with tin was studied in the ASDEX Upgrade (AUG) outer divertor. The CPS module was flush mounted as part of a target tile and exposed using the AUG divertor manipulator. In order to predict tin erosion from the designed module under typical AUG divertor loading conditions, the experiment was interpreted using the HeatLMD code. Preceding test exposures of the CPS in the high heat flux facility GLADIS were performed and interpreted by modelling to quantify the thermo-mechanical properties of the module. The results for the reference AUG discharge indicated a total of 2.6×10^{17} tin atoms (51 μg) would be eroded during the exposure, predominantly through temperature enhanced sputtering. The vapour cooling power was predicted to be negligible (5 kW/m^2 at the end of a 5 s exposure with heat flux from the plasma of 2 MW/m^2). The module was expected to be compatible with plasma operation, with tin erosion too low for any significant effect on the plasma performance. However, interpretative modelling of the experimental discharge with the highest exposure time yielded significantly lower tin erosion than observed. To be attributed to tin radiation the experimentally observed increase in total radiative power (1.5 MW) would require 2×10^{18} tin atoms (peak calculated erosion rate) radiating in the core plasma. This would require every tin atom eroded, to reach the core, which is unlikely.

Introduction

One of the most pressing issues in DEMO or a future fusion power plant construction is the heat load on the first wall and especially the divertor [1]. Plasma facing components based on liquid metal technologies could provide a solution to this problem. Capable of withstanding high heat fluxes (>15 MW/m^2 steady-state [2]), they could provide a viable replacement of the currently utilised solid tungsten-based components [3]. To successfully implement the technologies into designs of future fusion devices, a careful assessment of the performance of liquid metal plasma facing components in tokamak conditions is required. A key component of the viability assessment for future fusion devices is the performance of a liquid metal divertor (LMD) under ELMy H-mode plasmas where significant heat shocks, >60 MJm^{-2}s$^{-1/2}$ are expected [4].

For this reason, an experimental campaign was executed at the COMPASS tokamak with two LMD modules filled with Li and SnLi alloy exposed to ELMy H-mode plasmas [5]. Another suitable candidate for a liquid metal (tin), was not tested on COMPASS tokamak, as the performance capability of the device in terms of achievable power load and exposure duration was not optimal for such an experiment [6].

A dedicated experimental campaign at the ASDEX Upgrade tokamak (AUG) [8] was carried out with an additively manufactured tungsten CPS filled with tin. The objective was to expose the module to diverted L-mode and ELMy H-mode plasmas ($q_\perp \approx$ 3-5 MW/m², t = 2-3.5 s), representing the first test of a Sn-filled test module at the strike point of a diverted tokamak plasma. This was preceded by a test of the module at the high heat flux facility GLADIS [9] ($\dot{q}$ = 2-8 MW/m², t = 2.5-10 s) to confirm the compatibility of the module with AUG divertor plasma conditions before tokamak exposure.

Sn-filled module

A 40x16x25 mm³ (Fig. 1c) additively manufactured tungsten capillary porous structure (CPS) was installed flush-mounted in a customized divertor tile on a probe head of the AUG divertor manipulator [10] for exposure at the outer divertor target of AUG. The module consists of two parts. At the top is the actual 1.5 mm thick CPS layer with a porosity ε_{CPS} = 0.37 and pore and grain sizes <30 µm. The volume of the CPS layer would have technically allowed the infiltration of 2 g of tin. However, this was reduced to 1.5 g of tin to prevent potential excessive spill of liquid tin under high heat load. The bottom 23.5 mm part was made from solid (but also additively manufactured) tungsten with a porosity of ε_{bulk} = 0.12. Because of the manufacturing process the corresponding material parameters (heat capacity and conductivity) were expected to deviate from those of conventional tungsten [11], and a dedicated measurement was required to obtain them together with those of the CPS layer.

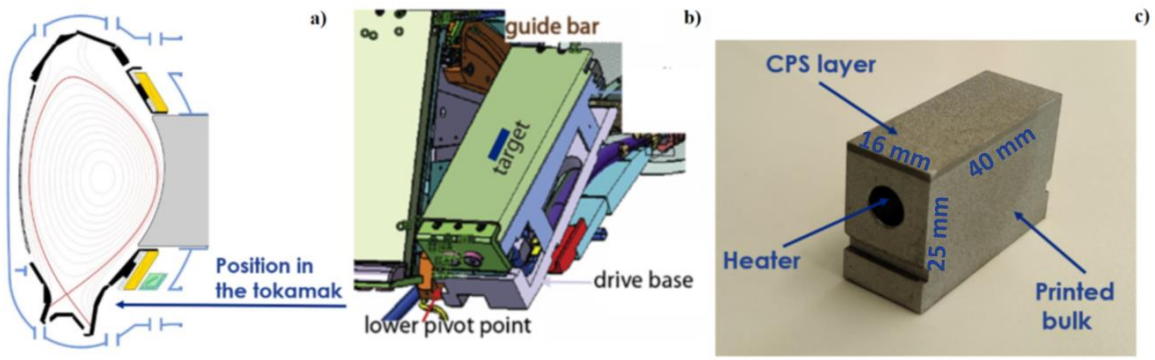

Fig. 1: Schema of the experimental setup: a) Position of the module in the tokamak. b) Outer divertor port manipulator with the position of the module highlighted, edited from [10]. c) Photograph and description of the module.

High Heat flux loading in GLADIS

Before being exposed to AUG plasma discharges the module was tested at the high heat flux facility GLADIS [9]. This was required to confirm the compatibility of the module with AUG divertor plasma conditions, both in tin-wetted and unwetted condition, as well as for quantifying the material parameters of the module. The wetted module was exposed to a total of 19 discharges with varying heat fluxes and times ($\dot{q}$ = 2-8 MW/m², t = 2.5-10 s). Pulse #264327 ($\dot{q}$ = 4 MW/m² and t = 7.5 s) was chosen for the benchmark modelling because of optimal heat deposition and diagnostics data (IR camera and pyrometer).

According to [12] the heat conductivity of a porous material can be calculated as $\kappa_{por} = \kappa\frac{1-\varepsilon}{1+11\varepsilon^2}$ where κ is the conductivity of the pure material and ε is the porosity. For tungsten with ε_{bulk} = 0.12 and κ_W = 130 W/m/K [12], the conductivity of the bulk should be κ_{bulk} = 99 W/m/K. In this calculation, the specific material properties of additively manufactured tungsten were not considered, which could result in a slightly lower conductivity.

For porous materials wetted with a fluid heat conductivity can be calculated as $\kappa_{fill} = \kappa_s \frac{1-\left(1-\frac{b\kappa_f}{\kappa_s}\right)\varepsilon}{1+(b-1)\varepsilon}$ where κ_f is the conductivity of the fluid and κ_s is the conductivity of the solid and $b = \frac{3\kappa_s}{(2\kappa_s+\kappa_f)}$ [13]. For a tungsten CPS with porosity ε_{CPS} = 0.37 and conductivity of tin κ_{Sn} = 26 W/m/K [13] the resulting conductivity of the CPS layer should be κ_{CPS} = 84 W/m/K. Volumetric heat capacities of the CPS C_{vCPS} =2.2 MJ/m^3/K and bulk C_{vbulk} = 2.3 MJ/m^3/K were calculated using the rule of mixture, i.e. C_v = (1- ε)C_{vW} + (0.8 εC_{vSn}) with C_{vW} = 2.57 MJ/m^3/K and C_{vSn} = 1.65 MJ/m^3/K [13].

The factor 0.8 is attributed to the underfilling of the CPS. In case of heat conductivity, the tungsten structure is the primary part determining the CPS heat conductivity. We omit the filling factor of 0.8 for the heat conductivity calculation as it is not clear if this simple approach is valid. Taking it onto account would increase/decrease the conductivity by 3.5%. All heat conductivities and capacities are calculated as temperature dependent.

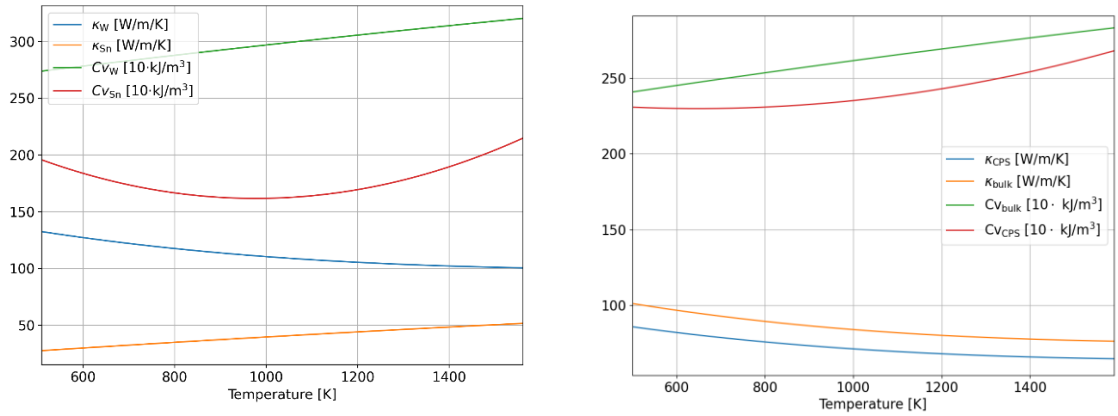

Fig. 2: Temperature dependency of W and Sn heat capacity and conductivity (left) and calculated heat conductivity and volumetric capacity of the CPS and bulk (right).

Modelling of GLADIS results in HeatLMD

The HeatLMD code, described in detail in [6,7], is a 3D plus temporal code for liquid metal surface and plasma interaction. It consists of a finite element solution of the heat equation, surface erosion (physical and thermal sputtering and evaporation) and subsequent vapour cooling effect. The inputs into the code are relevant plasma parameters at the target surface (electron temperature and density, impacting ion flux and energy, perpendicular heat flux, magnetic field strength) and the main outputs are the erosion rate, vapour cooling power and the surface temperature.

2D modelling of the module surface temperature evolution during the GLADIS pulse #264321 ($\dot{q}$= 4 MW/m^2 and t = 7.6 s) was done in the HeatLMD code, to validate the estimated heat conductivities and heat capacities of the CPS and the bulk of the module. 3D modelling is not required in this case as homogenous heating of the module can be assumed. As seen in Fig. 3 the computed surface temperature closely matches the experimental data during the heating phase t = 2.5-10.1 s, whereas during the cooling phase (t >10 s) there is a significant deviation. A possible cause of the deviation might be a reduced thermal contact between the CPS and the W target (see Fig. 1b), which is not currently considered in the model. Therefore, a more in-depth analysis is required. The closely matching temperatures at t = 20 s (simulated module in thermal equilibrium) suggest the estimation of the volumetric heat capacity (total thermal energy in the module) was correct. The surface temperature of the module decreased further after t = 20 s because of the thermal contact with the support structure, which the model did not consider.

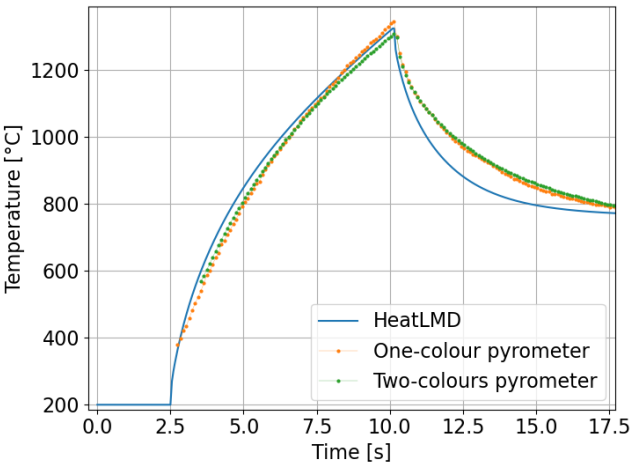

Fig. 3: LMD module surface calculated by HeatLMD and compared to the pyrometrical measurements. The one-colour pyrometer (orange) was corrected with ε=0.25.

No substantial change in the surface temperature evolution over time during simulation runs with various heat conductivities (in the range of 42-100 W/m/K) of the CPS layer was observed. The insensitivity of the model with respect to this parameter implies that the estimation by the modelling has a significant error (+/-50 %). The likely reason was a combination of thinness of the CPS layer and the presence of a drilled hole for installation of an electrical heater element. Because the hole was empty during the GLADIS experiment, it served as a thermal break, decreasing the effective heat transport between the centre of the surface and the bulk material (See Fig. 4). The top part of the module therefore had almost constant temperature from the surface to the depth of the hole over the main part of the discharge, thus, strongly reducing the effect of the heat conductivity near the surface. The peak temperature difference between cases with $\kappa = 98$ W/m/K (the conductivity of the bulk), and $\kappa = 42$ W/m/K, half of the expected value, was 75 °C (6% difference). The expected value of $\kappa = 84$ W/m/K was therefore chosen for all following calculations.

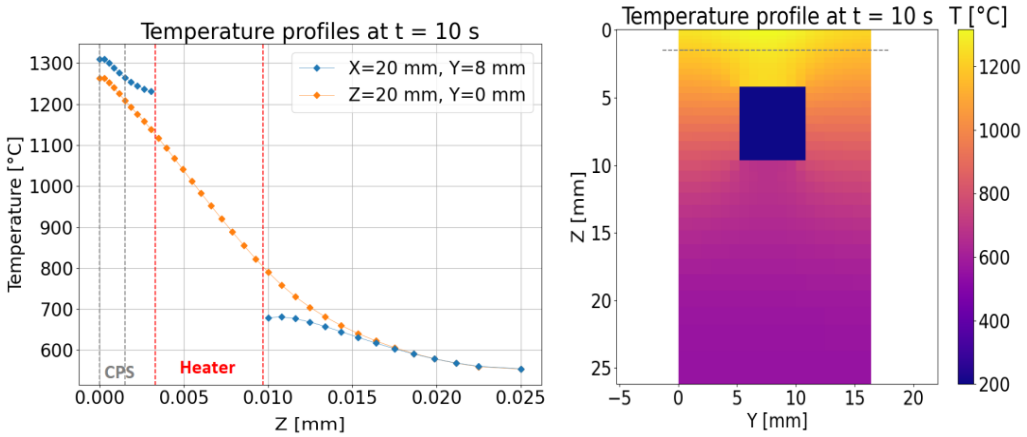

Fig. 4: Calculated temperature profiles of the GLADIS discharge at t = 10 s in the middle (Y = 8 mm) and at the edge (Y = 0 mm) of the target (left) and a 2D profile (right), indicating the conduction suppression effect of the heater hole.

The current structure of the HeatLMD code does not allow for a circular heater hole to be implemented, however, the square profiled geometry, used in the simulations, was validated by cross-checking with ANSYS modelling with correct geometry (circular hole).

ASDEX Upgrade LMD experiment setup

During the discharges, the outer strike-point was initially positioned above the target and then moved down on the CPS surface area for a set time interval and then raised up again to its initial position for plasma ramp down. The exposure interval was increased in subsequent discharges from 0.5 s up to 3.5 s. The time intervals in which the CPS was kept in the private flux region of the divertor with insignificant power flux levels were used to obtain in-situ reference data for the effect of the additional Sn source on plasma performance as well as reference data for surface temperature measurements by IR thermography. Moreover, camera inspection of the probe head surface in between discharges was used to obtain visual cues for Sn erosion effects on the plasma performance. The internal temperature

of the test module was monitored by two thermo-couples inserted in holes of different depth (3 mm and 8 mm below the surface).

ASDEX Upgrade modelling in HeatLMD

In order to find the optimal operation scenario for the experiment, a reliable prediction of tin erosion is highly beneficial. The desired scenario for this experiment should provide sufficient tin erosion to cause changes in plasma parameters, most notably total radiation, but not enough to cause radical changes and potentially plasma disruption. Another key aspect is the tin budget. Since there is no reservoir to replenish the eroded tin in the CPS, the experiment would have to be terminated prematurely if all the tin was lost from the CPS. Apart from a sudden drop in the tin source, there was no means of detecting the total loss of tin from the module, further increasing the importance of the reliable erosion prediction.

Two scenarios for predictive runs and an actual discharge from the experiment were selected for modelling (all ELMy H-mode). The objective of the predictive modelling was to investigate expected and high-power scenarios. The modelling of the actual discharge was done to interpret the observations from the experiment. The HeatLMD code, described in [6,7], with the addition of a runtime calculation of tin prompt redeposition was used for the erosion modelling. The HeatLMD model includes 3D and time evolving solution of the heat conduction in the module, liquid metal erosion (sputtering and evaporation) and vapour cooling (latent heat, collisional excitation and excitation processes). The heating element part, empty hole in the GLADIS case, made from a nichrome wire, implemented as a homogenous block of nichrome, had a time independent heat conductivity of 11.3 W/m/K and volumetric heat capacity 3.17 MJ/m^3/K [15]. The prompt redeposition fraction was calculated via a simple Monte Carlo approach. The approach was chosen to be simple enough to be utilizable during runtime of the simulation yet giving sufficiently representative results, over a constant value, which was the case in HeatLMD up until now [6,7]. Every timestep a set of escaping tin atoms with normally distributed kinetic energy is generated (typically around 10^4) in each element, enough to provide statistically precise results while not being computationally demanding. Each atom has an ionization mean free time, based on the measured plasma parameters (T_e, n_e) and the normal to surface velocity $v_\perp$ given by its energy (based on the surface temperature) and scattering launch angle (cosine distribution). The ionization mean free time is calculated as $t_i = rnd/(n_e < v\sigma >)$, where rnd is a random number from the interval [0,1). The ionization rate coefficients (in Fig. 5) were calculated in BIT1D code [16] from atomic data presented in [17]. Like tungsten, tin can be subjected to multiple ionizations within the sheath region, therefore the sheath electric potential is the dominant contributor to prompt redeposition over the gyromotion.

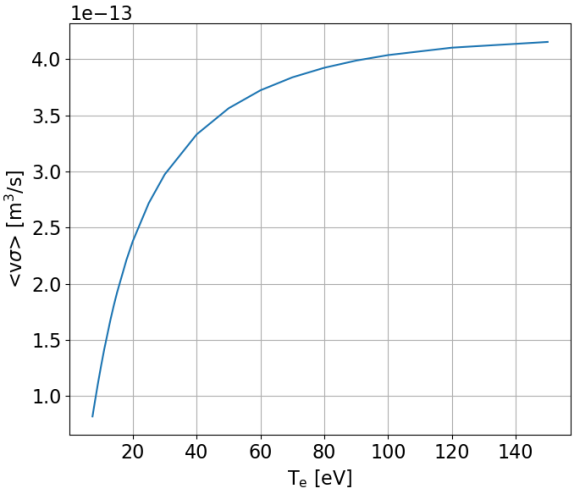

Fig. 5: Tin ionization rate coefficient as a function of electron temperature. Calculated in BIT1D [16] from data in [17].

If the atom is ionized within the magnetic presheath, it promptly redeposits. The border of the prompt redeposition layer was set as five times the Larmor radius of deuterium ions i.e. $l_i = v_\perp t_i < \frac{5\sqrt{5/2 T_e m_D k_B}}{B_t}$ yields prompt redeposition, according to the results of comprehensive kinetic modelling of tungsten redeposition in [18]. The prompt redeposition fraction is then given as the fraction of promptly redeposited atoms from the randomly generated set.

Firstly, the reference discharge scenario was simulated for validation, with two initial temperatures of the LMD considered (230 °C and 400 °C). Furthermore, a hypothetical discharge with significant power deposited on the target was used to simulate a 5 s of LMD exposure in vapour cooling regime. Finally, the discharge from the actual experiment with the longest exposure time of the module (3.5 s) was analysed. For the hypothetical highest power available scenario only the T_0 = 400 °C case was considered. For the experimental discharges the initial temperature was adjusted to T_0 = 230 °C by the CPS heating element. The plasma parameters of the modelled scenarios are listed in Table 1.

			Inter-ELM			ELM		
Disch. num.	Type	Exposure time [s]	T_e [eV]	n_e [10^{19}m^{-3}]	$q_\perp$ [MW/m^2]	T_e [eV]	n_e [10^{19}m^{-3}]	$q_\perp$ [MW/m^2]
38988	Reference	5	20	3.2	2	300	3.5	17
36663	Hypothetical	5	40	3.5	6	730	4	45
41279	Experimental	3.5	23	3.5	3	390	4	15

Table 1: Typical target plasma parameters at the strike point of the modelled discharges.

The perpendicular heat flux was taken from the IR camera measurements. The resolution of the camera is 0.66 ms in time and 0.58 mm per pixel in space [19]. Electron temperature and density were taken from the AUG triple probe array. The temporal resolution of the probes is 45 µs and the spatial resolution is 2.5 cm (at the location of the module). Because of the bias voltage of the probes being too low, the probes cannot measure valid electron temperatures during ELMs. The target electron temperature during ELMs was taken as 0.7 of the pedestal electron temperature obtained from the integrated data analysis (IDA) [20], consistently with results on JET [21].

Discharge number	Initial temperature [°C]	Maximal surface temperature [°C]	Eroded atoms [10^{17}]	Eroded mass [mg]	Prompt redeposition
38988	230	600	2.6	0.051	0.75
38988	400	770	6.3	0.124	0.75
36663	400	1900	1e5	1971	0.87
41279	230	980	17	0.335	0.77

Table. 2: Resulting maximal surface temperature, erosion, and average prompt redeposition at peak erosion point of the modelled discharges.

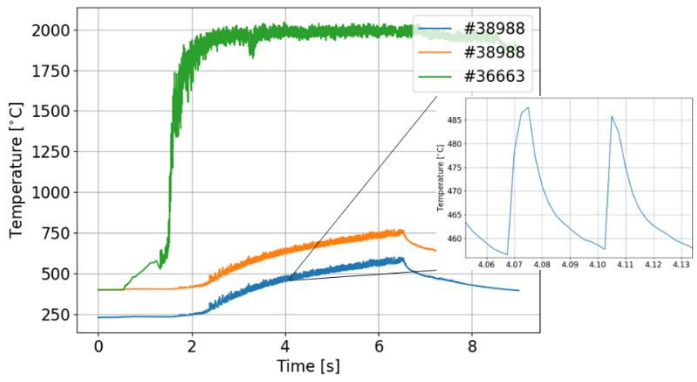

Fig. 6: Maximal surface temperature evolution for the predictive modelling scenarios.

The resulting maximal surface temperatures and erosions are listed in Table 2. The temperature evolutions of the modelled scenarios are shown in Fig. 6. The predicted peak surface temperature for the reference discharge of 590 °C (with T_0 = 230 °C) is well below the limit for significant tin erosion (through evaporation) >1000 °C [21], resulting in a total of 2.6x10^{17} of eroded atoms escaping into the divertor plasma. As expected, the maximal surface temperature of the T_0 = 400 °C scenario is 170 °C higher (the temperature curve is essentially shifted upwards) resulting in a 140 % increase of total tin erosion. Nevertheless, the higher value of 6.3x10^{17} tin atoms still would not have a significant effect on the plasma discharge. In both scenarios the dominant erosion effect is the thermally enhanced sputtering. In contrast, for the hypothetical high-power scenario the code predicts a release of 1x10^{22} tin atoms (2 g) into the divertor plasma over the

discharge, sufficient to greatly affect the discharge by corresponding radiation losses, likely even causing a radiative collapse. In case of the hypothetical scenario the so-called vapour shielding regime (where tin radiation prevents further heating of the surface) would be achieved after around a second of plasma exposure, with temperature locked at 1900 °C. This effect is typically observed at temperatures >1600 °C [22,23]. The exact value of the temperature lock depends not only on the heat flux but also on the plasma parameters (n_e, T_e), which determine the radiative cooling energy per one particle (i.e., how many radiating atoms are needed to dissipate a specific power).

Experiment modelling and data analysis

A new IR camera view observing the divertor manipulator is used to infer the temperature. This camera observes the divertor through a mirror on the high field side with a wide-angle view. It measures in the wavelength range of 3.5 µm to 5 µm. An emissivity of 0.15 is assumed. With the given spatial resolution, only a few pixels were observing the module surface. The view has a spatial resolution of 3mm/pixel and a time resolution of 1.7 ms in the present experiments. Therefore, comparison of surface temperature evolution between the simulation and experimental data was not trivial. Although the data do show a correlation (See Fig. 7), the deviation is notable. Especially between t = 4-6 s, where the rate of temperature increase temporarily decreases. This occurs during the time where the strike point was at a constant location, therefore an unaccounted physical effect, such as a change in emissivity or the structure of the liquid tin and CPS surface, likely distorted the IR camera data. This could have been the case in the post exposure cooling phase as well. The sudden drops in measured temperature at t = 7 s and t = 8.5 s indicate that another reason for the deviation is present. Since only a few pixels of the IR system are positioned on the module, a potential artefact might be created by a shift of the camera line of sight during the measurements.

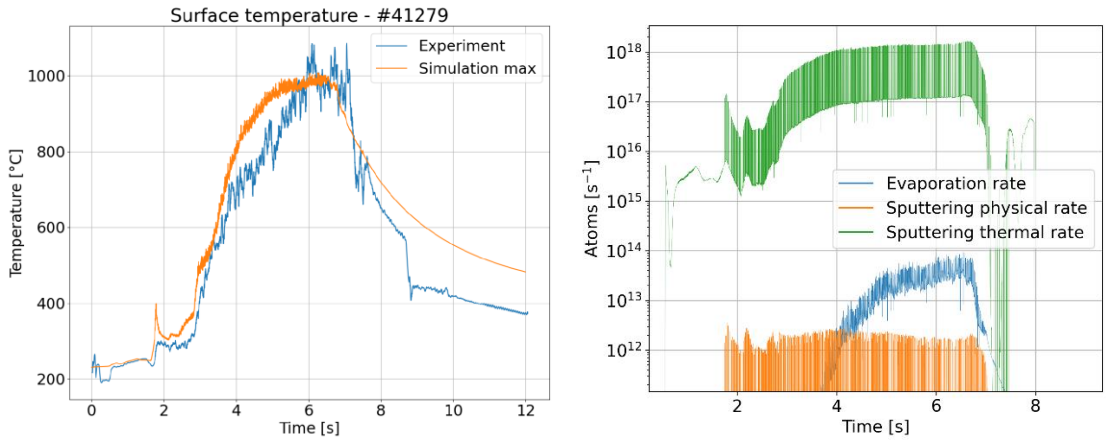

Fig. 7: Calculated and measured surface temperature (left) and calculated erosion rate from sputtering and evaporation (right) of the modelled experimental discharge #41279.

During the experimental discharge with the highest power and the longest exposure the surface temperature and plasma parameters were not sufficient to reach the vapour cooling regime. The drop in surface temperature increase at t = 4-6 s was most likely caused by a decrease of heat flux (measured by IR camera at a location 180° toroidally from the module), likely caused by an increase in radiation from the plasma. The vapour cooling power is <50 kW/m^2 (400 kW/m^2 during ELMs). Individual ELM heat shocks increased the surface temperature by ≈ 50 °C, comparable to the increase observed during the COMPASS experiment [6]. The increase in erosion during ELMs was (in peak) by an order of magnitude compared to the inter-ELM phase. The main cause was the increase in ion flux and impact energy.

During the experimental discharges with long LMD strike point exposure, a gradual increase in total radiation was observed, as can be seen in Fig. 8. In case of the modelled discharge, the increase was by 50% at the peak compared to discharges where the module was not exposed to the strike point.
The correlation of the radiation increase with the position of the strike point is apparent in Fig. 8. The outer strike point (OSP) is located above the module at the beginning of the discharge and is

subsequently shifted to approximately the middle of the module surface. In the period of constant OSP position, the total radiation gradually increases, corresponding to the steepest part of the surface temperature increase. After the strike point is moved back to its position above the module, the total radiation from the plasma begins to drop.

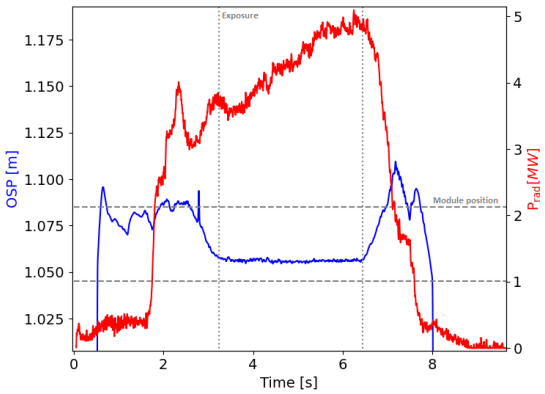

Fig. 8: Corelation of the increase in total radiation and the position of the strike point during discharge #41279.

This indicates, together with the fact that the increase was not observed during discharges with no exposure, that the excess radiation indeed originates from the tin contamination of the plasma.
The peak excessive radiation during discharge #41279 was P_{ex} =1.5 MW (50% increase).
The modelled peak erosion rate was 10^{17} atoms per second. This number of tin atoms could in principle radiate 1.5 MW if present in the core plasma, assuming radiation of 40 MeV/particle/s at T_e = 1 keV and n_e = 5x10^{19} m^{-3} [24]. However, this would require a very high percentage of the atoms (>90%) reaching the core plasma region, which is unlikely because of divertor impurity retention, e.g. presented in [25]. It has to be noted, that this estimate is arbitrary and serves only as an illustration, but the excessive need of impurity penetration mentioned earlier validates the general conclusion.

If the increase in total radiation cannot be explained by the erosion from sputtering and evaporation alone, another source of tin must have been present. There are two possible mechanisms currently deemed plausible. The first one is a tin leak located on the neighbouring tungsten manipulator tile which appeared already during one of the first discharges and not during the modelled one. The second is ejection of many tiny tin droplets from the surface of the module. Such an ejection was observed during an experimental campaign with a tin CPS at MAGNUM-PSI [26]. A planned follow-up experiment at MAGNUM-PSI [27] with the tested module could answer, whether it might have been the case for the AUG tested CPS as well. Ejection of just a few large droplets can be ruled out because it would lead to radiation spikes rather than the observed gradual increase. Which of these two mechanisms is responsible for the large increase remains to be validated.

Conclusion

A dedicated experiment with an LMD-mock-up consisting of an additively manufactured W CPS infiltrated with Sn was conducted at AUG. The module was exposed to both L-mode and ELMy H-mode plasmas. Preceding test exposures of the LMD module in the high heat flux facility GLADIS were modelled with the HeatLMD code to determine the thermo-mechanical material parameters of the module. The resulting parameters for the CPS layer are κ_{CPS} = 84 W/m/K, 2.2 MJ/m^3/K and for the module bulk material κ_{bulk} = 99 W/m/K and C_{vbulk} = 2.3 MJ/m^3/K. To predict tin erosion in plasma exposures, the HeatLMD code was used to simulate a reference discharge and a hypothetical high-power scenario with predicted total erosion of 2.6 x10^{17}, 6.3x10^{17} and 1x10^{22} tin atoms respectively. For interpretation of experimental data, also the discharge with the longest module exposure interval was simulated. The derived total number of tin atoms lost to the divertor plasma was 2x10^{18} atoms, dominantly by thermally enhanced sputtering. During the discharge with the longest exposure interval, a significant increase in total radiation was observed, not readily explainable by only tin sputtering and evaporation. Possible additional tin sources responsible for the excess tin in the plasma might be either a tin leak deposited at the adjacent tungsten tile surface in one of the first discharges, or ejection of many small droplets, or both. These would have been observable with a fast optical camera looking directly at the target and its vicinity with a sufficient spatial resolution. Further analysis of the underlying processes is required to resolve the discrepancy. Follow up experiment on MAGNUM-PSI is planned to help answer the remaining questions.

Acknowledgements

This work was conducted with the support of the Czech Science Foundation project GACR 22-03950S.

This work has been carried out within the framework of the EUROfusion Consortium, funded by the European Union via the Euratom Research and Training Programme (Grant Agreement No 101052200 —EUROfusion). Views and opinions expressed are however those of the author(s) only and do not necessarily reflect those of the European Union or the European Commission. Neither the European Union nor the European Commission can be held responsible for them.

References

[1] J. H. You, *et al.*, 2022, Fus. Eng. Des. **175** 113010
[2] T. W. Morgan. *et al.*, 2017, Nucl. Mat. Energy **12** 210-215
[3] F. L. Tabares, *et al.*, 2017, Nucl. Fusion **57** 016029 (11pp)
[4] T, Eich, *et al.*, 2017, Nucl. Mat. Energy **12** 84-90
[5] R. Dejarnac, *et. al.*, 2020, Nucl. Mat. Energy **25** 100801
[6] J. Horacek, *et al.*,2020, Nucl. Mat. Energy **25** 100860
[7] J. Horacek, et al. 2021, Phys. Scr. **96** 124013
[8] H. Meyer, *et al.*, 2020 Nucl. Fusion **59** 112014
[9] H. Greuner, *et al.*, 2007 J. Nuc. Mat. 367-370 1444-1448
[10] A. Herrmann, *et al.*, 2015, Fus. Eng. Design **98-99** 1496-1499
[11] A. E. Gheribi, *et al.*, 2015, Appl. Phys. Lett. **107** 094102
[12] J. C. Y. Koh and A. Fortini, 1973 Int. J. Heat Mass Transf. **16** 2013-1022
[13] W. Woodside, 1958, Can. J. Phys. **36** 815
[14] R. W. Powell, C. Y. Ho and P. E. Liley, 1966, Nat. Bur. Stand. Thermal Conductivity of Selected Materials
[15] P. Majumder and A. Bhattacharyya, 2008, Modelling Simul. Mater. Sci. Eng. **16** 015006
[16] D. Tskhakaya, *et al.*, 2013, J. Nuc. Mat. **438** 522-525
[17] R. Naghma, *et al.*, 2011, J. Phys. B: At. Mol. Opt. Phys. **44** 105204
[18] D. Tskhakaya,*et al.*, 2015, J. Nuc. Mat. **463** 624-628
[19] B. Sieglin, *et al.*, 2015, Rev. Sc. Inst. **86** 113502
[20] R. Fischer, *et. al.*, 2017, Fus. Sc. Tech. **58** 675-684
[21] J. Adamek, *et al.*, 2020, Nucl. Fusion **60** 096014
[22] T. W. Morgan, *et al.*, 2018, Plasma Phys. Control. Fusion **60** 014025
[23] G. Mazzitelli, *et al.*, 2019, Nucl. Fusion **59** 096004
[24] H. K. Chung, *et al.*, 2005, High En. Dens. Phys. **1** 3-12
[25] A. Geier, *et al.*, 2002, Plasma Phys. Control. Fusion **44** 2091-2100
[26] W. Ou, *et al.*, 2021, Nucl. Fusion **61** 066030
[27] G. De Temmerman, *et al.*, 2013, Fus. Eng. Design **88** 483-487